

Self-Assembly of Lamellar- and Cylinder-Forming Diblock Copolymers in Planar Slits: Insight from Dissipative Particle Dynamics Simulations

Pavel Petrus,[†] Martin Lísal,^{*,†,‡} and John K. Brennan[§]

[†]Department of Physics, Faculty of Science, J. E. Purkinje University, Ústí n. Lab., Czech Republic,

[‡]E. Hála Laboratory of Thermodynamics, Institute of Chemical Process Fundamentals of the ASCR, v. v. i., Prague 6-Suchdol, Czech Republic, and [§]U.S. Army Research Laboratory, Weapons and Materials Research Directorate, Aberdeen Proving Ground, Maryland 21005-5066

Received July 2, 2010. Revised Manuscript Received August 9, 2010

We present a dissipative particle dynamics simulation study on nanostructure formation of symmetric and asymmetric diblock copolymers confined between planar surfaces. We consider symmetric and slightly asymmetric diblock copolymers that form lamellar nanostructures in the bulk, and highly asymmetric diblock copolymers that form cylindrical nanostructures in the bulk. The formation of the diblock copolymer nanostructures confined between the planar surfaces is investigated and characterized by varying the separation width and the strength of the interaction between the surfaces and the diblock copolymers. Both the slit width and the surface interaction strongly influence the phase diagram, especially for the asymmetric systems. For the symmetric and slightly asymmetric diblock copolymer systems, the confinement primarily affects the orientation of the lamellar domains and only marginally influences the domain morphologies. These systems form parallel lamellar phases with different number of lamellae, and perpendicular and mixed lamellar phases. In a narrow portion of the phase diagram, these systems exhibit a parallel perforated lamellar phase, where further insight into the appearance of this phase is provided through free-energy calculations. The confined highly asymmetric diblock copolymer system shows, in addition to nanostructures with parallel and perpendicular cylinders, noncylindrical structures such as parallel lamellae and parallel perforated lamellae. The formation of the various confined nanostructures is further analyzed by calculating structural characteristics such as the mean square end-to-end distance of the diblock copolymers and the nematic order parameter.

1. Introduction

Diblock copolymers are formed by two chemically incompatible blocks A and B that are covalently bonded. Because of the covalent bonding, the A- and B-blocks cannot form separate phases when the diblock copolymers are quenched below the order-disorder temperature. Instead, the diblock copolymers self-assemble into nanostructures that minimize contacts between the A- and B-blocks. The shape of the nanostructure domains formed by the A- and B-blocks depends on the asymmetry of the diblock copolymers and the strength of chemical incompatibility between the blocks. In the bulk, diblock copolymers form four classical microphases, the lamellar phase for symmetric or slightly asymmetric diblock copolymers, and the cylindrical, gyroid, and micellar phases otherwise.¹ However, when confined in planar slits, adsorption interactions, symmetry breaking, structural frustration, and confinement-induced entropy loss influence the morphology of the nanostructure domains, where transitions into nanostructures not found in the bulk are possible. Moreover, diblock copolymers confined between two planar surfaces offer better control of nanostructure morphology and microdomain uniformity with respect to the bulk.² The natural tendency of diblock copolymers to self-organize into dense, regular arrays of nanostructures, either in bulk or confined environments, make them attractive materials for various nanotechnology-related applications.³

Our understanding of the self-assembly of symmetric and asymmetric diblock copolymer systems confined in planar slits

continues to deepen via experimental, theoretical, and simulation studies.^{4–6} The spatial scales of the structures make them amenable to relatively simple experimental setups, which has led to extensive laboratory studies (see Xiang et al.⁴ and references therein). Both confinement between parallel walls and within cylindrical pores have been studied experimentally, where in the latter case the pore curvature can strongly influence the morphology.⁴ Most theoretical studies have been based on the self-consistent mean-field theory (SCMFT),^{7,8} the cell dynamic system (CDS) method,⁹ the interfacial statistical associating fluid theory (iSAFT)¹⁰ and the dynamic density functional theory (DDFT).¹¹ A few notable theoretical studies are the works of Matsen,¹² Geisinger et al.,¹³ and Miao et al.¹⁴ who used the SCMFT to explore the interplay of the surface field with the incommensurability effect and nature of phase transitions for symmetric diblock copolymers in a slit geometry. Also worth noting are the CDS works of Feng et al.^{15,16} who studied the microphase separation and morphology of symmetric and slightly

- (4) Xiang, H.; Shin, K.; Kim, T.; Moon, S.; McCarthy, T. J.; Russell, T. P. *J. Polym. Sci., Part B: Polym. Phys.* **2005**, *43*, 3377–3383.
(5) Binder, K. *Adv. Polym. Sci.* **1999**, *138*, 1–89.
(6) Fasolka, M. J.; Mayes, A. M. *Annu. Rev. Mater. Res.* **2001**, *31*, 323–355.
(7) Edwards, S. F. *Proc. Phys. Soc., London* **1965**, *85*, 613–624.
(8) Helfand, E. *J. Chem. Phys.* **1975**, *62*, 999–1005.
(9) Oono, Y.; Puri, S. *Phys. Rev. A* **1988**, *38*, 434–453.
(10) Jain, S.; Chapman, W. G. *Mol. Phys.* **2009**, *107*, 1–17.
(11) Fraaije, J. G. E. M.; van Vlimmeren, B. A. C.; Maurits, N. M.; Postma, M.; Evers, O. A.; Hoffmann, C.; Altevogt, P.; Goldbeck-Wood, G. *J. Chem. Phys.* **1997**, *106*, 4260–4269.
(12) Matsen, M. W. *J. Chem. Phys.* **1997**, *106*, 7781–7791.
(13) Geisinger, T.; Müller, M.; Binder, K. *J. Chem. Phys.* **1999**, *111*, 5241–5250.
(14) Miao, B.; Yan, D.; Wickham, R. A.; Shi, A.-C. *Polymer* **2007**, *48*, 4278–4287.
(15) Feng, J.; Liu, H.; Hu, Y. *Macromol. Theory Simul.* **2002**, *11*, 549–555.
(16) Feng, J.; Liu, H.; Hu, Y. *Macromol. Theory Simul.* **2002**, *11*, 556–565.

*To whom correspondence should be addressed. E-mail: lisal@icpf.cas.cz.

(1) Bates, F. S.; Frederickson, G. H. *Annu. Rev. Phys. Chem.* **1990**, *41*, 525–557.
(2) Shin, D. O.; Kim, B. H.; Kang, J.-H.; Jeong, S.-J.; Park, S. H.; Lee, Y.-H.; Kim, S. O. *Macromolecules* **2009**, *42*, 1189–1193.

(3) Xia, Y.; Rogers, J. A.; Paul, K. E.; Whitesides, G. M. *Chem. Rev.* **1999**, *99*, 1823–1848.

asymmetric diblock copolymers confined in slits with neutral and attractive surfaces. The iSAFT¹⁰ has been used to study the effect of confinement on the ordering of symmetric diblock copolymers relative to the confining walls. Similarly, DDFT has been utilized, for example, by Huinink et al.^{17,18} for the prediction of the phase diagram of asymmetric diblock copolymers confined in slits with surfaces exhibiting different affinity to the copolymer blocks. Most simulation studies employed a lattice Monte Carlo method with the primary aim of supporting the theoretical findings.^{15,16,19} Recently, we carried out a systematic study of symmetric diblock copolymers in slits with and without nanopatterns using dissipative particle dynamics (DPD) simulations.²⁰ We observed novel nanostructures in the nanopatterned slits and we attempted to rationalize their self-assembly based on the behavior we observed in the slits without nanopatterns.

In the theoretical and simulation studies mentioned above, each slit wall typically has a substantial preferential affinity toward one of the blocks. For symmetric or slightly asymmetric diblock copolymers, this preferential affinity mostly results in lamellae aligning in a parallel orientation with respect to the walls. Ideally, the parallel lamellar phase adopts lamellae of thickness vW_{LAM}^0 , where v is an integer corresponding to the number of lamellae and W_{LAM}^0 is the bulk phase lamellar spacing.²¹ In cases where the natural spacing of the lamellae is incommensurate with the slit width W , that is, $W \neq vW_{\text{LAM}}^0$ for any value of v , a parallel lamellar phase becomes energetically and structurally frustrated. To avoid this situation, the lamellae prefer to align perpendicular to the walls. While a perpendicular lamellar phase cannot accommodate the energetically favorable layering of the preferentially adsorbed block, its lamellae spacing is free to relax to its bulk phase spacing. For slightly asymmetric diblock copolymers confined in slits, lamellae can also orientate to a mixed lamellar phase, either with v parallel lamellae adsorbed at one surface and perpendicularly orientated lamellae at the other surface, or with parallel lamellae adsorbed at both surfaces and perpendicularly orientated lamellae between these lamellae. Although the presence of an interface between the two lamellae orientations is energetically costly, this cost is compensated by the adsorbed layer(s) at the wall(s).^{12,22} For these cases of confined symmetric or slightly asymmetric diblock copolymers, the affinity of the blocks toward the walls primarily affects the orientation of the nanostructure domains but not the shape of the domains. For *asymmetric* diblock copolymers confined in the slits, the preferential wetting of the surfaces by one of the blocks leads to not only parallel and perpendicular orientations of cylinders, but also causes transitions to non-cylindrical nanostructures such as parallel lamellae or parallel perforated lamellae.^{17,18}

In this work, we use the DPD method to explore spontaneous nanostructure formation of lamellar- and cylinder-forming diblock copolymers confined between planar surfaces, where the surfaces are modeled as dense layers of DPD beads. The self-assembly is characterized by varying the slit width and the interaction between the walls and the copolymer blocks. Qualitative phase diagrams are presented for these systems along with the corresponding conformational and order parameter behavior

of the diblock copolymers. We make no attempt to locate precise phase boundaries separating the different nanostructures, rather we attempt to quantify the various effects on the self-assembly. We consider symmetric, slightly asymmetric, and asymmetric diblock copolymer systems. For the symmetric case, we continue from our previous work²⁰ focusing here on the formation of the parallel perforated lamellar phase that was discovered in a narrow portion of the phase diagram, where insight into the occurrence of this phase is provided by free-energy calculations.

2. Simulation Methodology

In this work, the DPD method is used, where all details regarding the method and the confined diblock copolymer models can be found in the Appendix. Also described in the Appendix is a procedure for top-down mapping of the diblock copolymer models onto real systems.

2.1. Phase Morphology and Chain Structure Properties. Following convention for DPD copolymer simulations, the types of phase morphologies are primarily identified by visual inspection of the simulation snapshots, where we used both bead representations and A-B dividing surfaces. The dividing surface representation corresponds to a plane of constant density equal to $[n/(n+m)]\rho$, where n and m are the number of A- and B-beads in the diblock copolymer, respectively, and ρ is the bead density. In addition, the calculation of density profiles of A- and B-beads and chain conformation properties complemented the identification of the phase morphology. On the phase diagram, approximate boundaries between microphase separated regions were then indicated as lines between adjacent points that exhibited the different morphologies. This visual inspection approach is routinely used in DPD and DDFT studies for determining phase diagrams, see, for example, refs 17, 18, and 23–25.

The following structural properties were evaluated to deduce the conformational and order parameter behavior of the diblock copolymers in the slits. Density profiles of A- and B-beads, $\rho_\alpha(z)$, characterize the structure of the diblock copolymers in the direction normal to the surface (z -direction). For $\alpha = A$ or B , $\rho_\alpha(z)$ is given by

$$\rho_\alpha(z) = \left\langle \frac{1}{L_x L_y \Delta z} \sum_j H_n^\alpha(z_j) \right\rangle \quad (1)$$

where L_x and L_y are the lengths of the simulation box in the x - and y -directions, respectively, Δz is the slab width in the z -direction, $\langle \cdot \rangle$ denotes an ensemble average and $H_n^\alpha(z_j)$ is the top-hat function for the z -component of particle j , z_j , defined as

$$H_n^\alpha(z_j) = \begin{cases} 1 & z_n - \frac{\Delta z}{2} < z_j < z_n + \frac{\Delta z}{2} \\ 0 & \text{otherwise} \end{cases} \quad (2)$$

In typical fashion for A_nB_m diblock copolymer simulations, the mean square end-to-end distance

$$R_e^2 = \left\langle \frac{1}{N} \sum_{i=1}^N (\mathbf{r}_{1,i} - \mathbf{r}_{n+m,i})^2 \right\rangle \quad (3)$$

(23) Groot, R. D.; Madden, T. J.; Tildesley, D. J. *J. Chem. Phys.* **1999**, *110*, 9739–9749.

(24) Horsch, M. A.; Zhang, Z.; Iacovella, C. R.; Glotzer, S. C. *J. Chem. Phys.* **2004**, *121*, 11455–11462.

(25) Martinez-Veracoechea, F. J.; Escobedo, F. A. *J. Chem. Phys.* **2006**, *125*, 104907.

(17) Huinink, H. P.; Brokken-Zijp, J. C. M.; van Dijk, M. A.; Sevink, G. J. A. *J. Chem. Phys.* **2000**, *112*, 2452–2462.

(18) Huinink, H. P.; van Dijk, M. A.; Brokken-Zijp, J. C. M.; Sevink, G. J. A. *Macromolecules* **2001**, *34*, 5325–5330.

(19) Kikuchi, M.; Binder, K. *J. Chem. Phys.* **1994**, *101*, 3367–3377.

(20) Petrus, P.; Lisal, M.; Brennan, J. K. *Langmuir* **2010**, *26*, 3695–3709.

(21) Ohta, T.; Kawasaki, K. *Macromolecules* **1986**, *19*, 2621–2632.

(22) Walton, D. G.; Kellogg, G. J.; Mayes, A. M.; Lambooy, P.; Russell, T. P. *Macromolecules* **1994**, *27*, 6225–6228.

and the mean square radius-of-gyration

$$R_g^2 = \left\langle \frac{1}{N} \sum_{i=1}^N \left[\frac{1}{n+m} \sum_{j=1}^{n+m} (\mathbf{r}_{j,i} - \mathbf{r}_{\text{com},i})^2 \right] \right\rangle \quad (4)$$

are used to define the characteristic size of a polymer chain. In eqs 3 and 4, N is the number of diblock copolymers, $\mathbf{r}_{j,i}$ is the position of bead j belonging to diblock copolymer i , and $\mathbf{r}_{\text{com},i}$ is the position of the center-of-mass of diblock copolymer i . Diblock copolymer chains confined in planar slits can be further characterized by the mean square radius-of-gyration parallel and perpendicular to the wall, $R_{g,\parallel}^2$ and $R_{g,\perp}^2$, respectively, which are given by the expressions

$$\begin{aligned} R_{g,\parallel}^2 &= \left\langle \frac{1}{N} \sum_{i=1}^N \left\{ \frac{1}{n+m} \sum_{j=1}^{n+m} [(x_{j,i} - x_{\text{com},i})^2 + (y_{j,i} - y_{\text{com},i})^2] \right\} \right\rangle \\ R_{g,\perp}^2 &= \left\langle \frac{1}{N} \sum_{i=1}^N \left[\frac{1}{n+m} \sum_{j=1}^{n+m} (z_{j,i} - z_{\text{com},i})^2 \right] \right\rangle \end{aligned} \quad (5)$$

where x,y,z are the Cartesian coordinates of r . Note that $R_g^2 = R_{g,\parallel}^2 + R_{g,\perp}^2$.

Finally, the nematic order parameter

$$P_{2,d} = \frac{3}{2} \langle \lambda_{\max} \rangle \quad (6)$$

is a convenient measure of orientational order.²⁶ In eq 6, λ_{\max} is the largest eigenvalue of the Sausse tensor

$$Q_{\alpha\beta} = \frac{1}{N} \sum_{i=1}^N e_{i,\alpha} e_{i,\beta} - \frac{\delta_{\alpha\beta}}{3} \quad (7)$$

where based on Einstein's vector notation \mathbf{e}_i is the unit vector with components $e_{i,\alpha}$ and $e_{i,\beta}$ along the end-to-end direction of diblock copolymer i , and $\delta_{\alpha\beta}$ is the Kronecker delta. $P_{2,d}$ is zero in a completely orientationally disordered state and is unity if the diblock copolymers are perfectly aligned.

2.2. Free-Energy Calculations. In this work, for symmetric diblock copolymer systems in which one of the blocks exhibits strong phobicity toward the surfaces, the parallel perforated lamellar phase existed in a narrow portion of the phase diagram and it evolved from the perpendicular lamellar phase. The phase transition between the perpendicular and parallel perforated lamellar morphologies is a first-order transition and is associated with the occurrence of metastable lamellar morphologies comprised of both perpendicular and parallel oriented lamellae. To provide further insight into the stability of these lamellar morphologies, we calculated the Helmholtz free energy as a function of the block-surface phobicity. These free-energy calculations are not intended as a means to determining phase co-existence. Rather, they are used to differentiate the most stable morphology for cases where multiple morphologies are observed at a single state point. In such cases, the most stable morphology exhibits the lowest Helmholtz free energy.

The DPD simulations were carried out at constant slit volume, constant temperature T and constant number of diblock copolymers, thus the Helmholtz free energy is the relevant thermodynamic

function. Moreover, the ideal-gas contributions to the Helmholtz free energy need not be considered since they are not affected by the change of the block-surface phobicity. Subsequently, the excess Helmholtz free energy F^{ex} can be expressed as^{27,28}

$$\beta F^{\text{ex}}(N, T, A, W) = N\beta\mu^{\text{ex}} - \beta\Pi^{\text{ex}}AW \quad (8)$$

where μ^{ex} is the configurational chemical potential and Π^{ex} is the excess spreading pressure (defined as the excess average mechanical pressure parallel to the slit walls), $\beta = 1/(k_B T)$, k_B is Boltzmann's constant and $A = L_x L_y$. (The equivalent terms lateral pressure and transverse pressure are also used in the literature.) Details regarding the determination of μ^{ex} and Π^{ex} are provided in the Appendix.

2.3. Computational Details. In this work, we used the following reduced units: the cutoff radius r_c is the unit of length, $k_B T$ is the unit of energy, and the mass of a DPD bead is the unit of mass. Using these reduced units, we set $\rho = 3$ (which corresponds to a dense polymer melt), the noise amplitude $\sigma_{ij} = 3$, the wall-bead tethering constant $K_w = 100$, and the time step $\Delta t = 0.03$. It was assumed that all bead types (polymer and wall) have the same mass, m_{DPD} . We investigated the behavior of diblock copolymers comprised of ten DPD beads with the following arrangements: (i) five A- and five B-beads, A_5B_5 (a symmetric diblock copolymer), (ii) four A- and six B-beads, A_4B_6 (a slightly asymmetric diblock copolymer), and (iii) three A- and seven B-beads, A_3B_7 (a highly asymmetric diblock copolymer). The maximum repulsion between beads A and B was set as $a_{AB} = 40$ with the spring constant $K_s = 4$ and equilibrium spring length $r_0 = 0$. Groot and Madden²⁹ have shown that these values of K_s and r_0 provide a reasonable description of the structural properties of bulk diblock copolymer melts at $\rho = 3$. We set $L_x = L_y = 25$ and varied the slit width W in the z -direction from 2 to 20 with unit steps. In some cases, we also employed different L_x and L_y to investigate finite-size and commensurate effects on the self-assembly, most typically for cases near or at the phase boundaries between different types of nanostructures. Specifically, we considered $L_x = 20$ and $L_y = 25$, and $L_x = 20$ and $L_y = 30$. Numerical integration of the DPD equations of motion was performed using the modified velocity-Verlet algorithm.³⁰ To improve computational efficiency, we implemented the cell linked list method for the energy and force calculations.^{31,32} Typically, production runs spanned 600 000 time steps, but for the free-energy calculations and for some simulations near the phase separation boundaries, as many as 6 000 000 time steps were used.

Simulations of the spontaneous formation of diblock copolymer nanostructures require employing a convenient strategy that reasonably guarantees the most stable structure will be found. In this work, we use the following conventional strategy based on a slow cooling of the diblock copolymers.²⁴ The values of a_{AB} were slowly increased from $a_{AB} = a_{AA}$, where $a_{AA} \equiv a_{BB} = 25$, to the target value of 40; this approach corresponds to a slow decrease in T . Each increase of a_{AB} was followed by a DPD simulation that allowed the system to relax to an equilibrated state. The increase of a_{AB} was typically performed with unit steps and with a relaxation period of 60 000 time steps.

(27) Forsman, J.; Woodward, C. E. *Mol. Phys.* **1997**, *90*, 637–652.

(28) Escobedo, F. A. *J. Chem. Phys.* **2001**, *115*, 5642–5652.

(29) Groot, R. D.; Madden, T. J. *J. Chem. Phys.* **1998**, *108*, 8713–8724.

(30) Groot, R. D.; Warren, P. B. *J. Chem. Phys.* **1997**, *107*, 4423–4435.

(31) Frenkel, D.; Smit, B. *Understanding Molecular Simulation: From Algorithms to Applications*, 2nd ed.; Academic Press: London, 2002.

(32) Allen, M. P.; Tildesley, D. J. *Computer Simulation of Liquids*, 2nd ed.; Clarendon Press: Oxford, 1987.

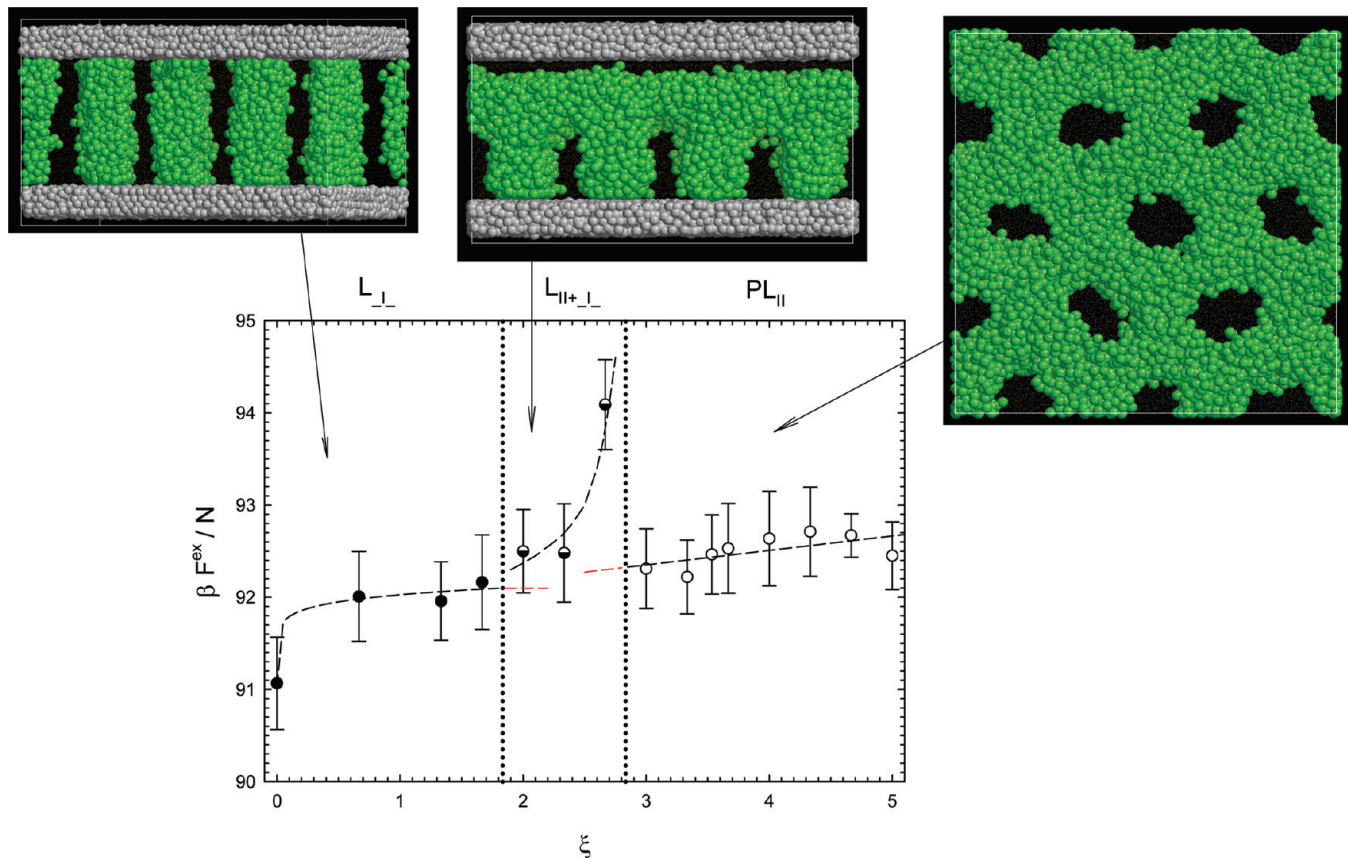


Figure 1. The excess Helmholtz free energy, F^{ex} , as a function of the phobicity ξ for the A_5B_5 system confined in planar slits of width 10. Symbols represent simulation results and vertical dotted lines denote approximate boundaries between the particular phases. $\beta = 1/(k_B T)$, T is the temperature, k_B is Boltzmann's constant, and N is the number of A_5B_5 copolymers. Dashed lines correspond to fits of the simulation results within each phase region, while red indicates extrapolations of the fits from the L_{\perp} and PL_{\parallel} regions into the $L_{\parallel+\perp}$ region. Error bars correspond to the standard deviations over three independent free-energy measurements. Also shown are examples of simulation configurations for the stable perpendicular (L_{\perp}), metastable mixed ($L_{\parallel+\perp}$), and stable parallel perforated (PL_{\parallel}) lamellar phases. Green and gray spheres represent A- and wall-beads, respectively. B-beads in all cases and wall-beads in the case of the PL_{\parallel} simulation configuration are not shown for visual clarity.

3. Results and Discussion

We carried out DPD simulations of the self-assembly of the A_5B_5 , A_4B_6 , and A_3B_7 copolymers in planar slits with W ranging from 2 to 20 with unit steps. We varied either a_{Aw} (the subscript w denotes the wall beads) while keeping $a_{Bw} = a_{AA}$, or a_{Bw} while keeping $a_{Aw} = a_{AA}$, where values ranged from 25 up to 80. The ratio $(a_{Aw} - a_{Bw})/\Delta a_{AB} \equiv \xi$, where $\Delta a_{AB} = a_{AB} - a_{AA}$, was used to characterize the phobicity of the A- and B-beads toward the walls. Thus in terms of ξ , the relative A- and B-bead repulsions can be categorized by the following: (i) $\xi = 0$, A- and B-beads have equal repulsion from the wall beads; (ii) $\xi > 0$, A-beads have a higher repulsion from the wall beads, where as ξ increases the A-wall bead repulsion increases; and (iii) $\xi < 0$, B-beads have a higher repulsion from the wall beads, where as ξ decreases the B-wall bead repulsion increases.

3.1. Symmetric Diblock Copolymers with High Phobicity toward the Walls. In previous work, we studied the details of the self-assembly of A_5B_5 copolymers confined between planar walls of varying separation width.²⁰ As part of the work presented in this study, we further investigate the self-assembly behavior of A_5B_5 copolymers in a particular slit width ($W = 10$), where in the present work we have discovered a parallel perforated lamellar phase (denoted as PL_{\parallel}). By increasing the block-wall phobicity, we observed a first-order transition from a perpendicular lamellar phase (denoted as L_{\perp}) into a PL_{\parallel} phase that was accompanied by

the occurrence of a metastable lamellar phase (denoted as $L_{\parallel+\perp}$) comprised of both parallel and perpendicular oriented lamellae.

At $W = 10$ only, we found that perpendicular lamellae are stable up to $\xi \approx 1.85$. Upon increasing ξ above 1.85, the L_{\perp} phase first transforms into a metastable $L_{\parallel+\perp}$, while further increasing ξ above 2.85, the system self-assembles into a stable PL_{\parallel} phase (see Figure 1 for examples of configuration snapshots of these morphologies). The simulations showed that the perpendicular and parallel perforated lamellar morphologies, in contrast to the mixed lamellar morphology, were formed regardless of the path that led the system to its final state. Namely, a L_{\perp} phase was spontaneously formed by the slow cooling protocol described in Section 2.3 (for $0 < \xi < 1.85$), while a L_{\perp} phase persisted when starting from perpendicular lamellae at $\xi = 0$ and increasing ξ up to 1.85. Likewise, the A_5B_5 copolymer system self-assembled into a PL_{\parallel} phase by the slow cooling strategy (for $2.85 < \xi < 5$), and also by transformation from perpendicular lamellae upon increasing ξ above 2.85. For all cases considered for both the L_x and L_y phases, this behavior was observed even when values of L_x and L_y were varied. However, for the $L_{\parallel+\perp}$ phase when different pathways were considered (including the cooling strategy (for $1.85 < \xi < 2.85$), the transformation from the L_{\perp} phase upon increasing ξ , the transformation from the PL_{\parallel} phase upon decreasing ξ , and varying L_x and L_y), the resulting mixed lamellar morphology varied. In particular, for many cases the lamellae in the slit were oriented differently, where in some instances they

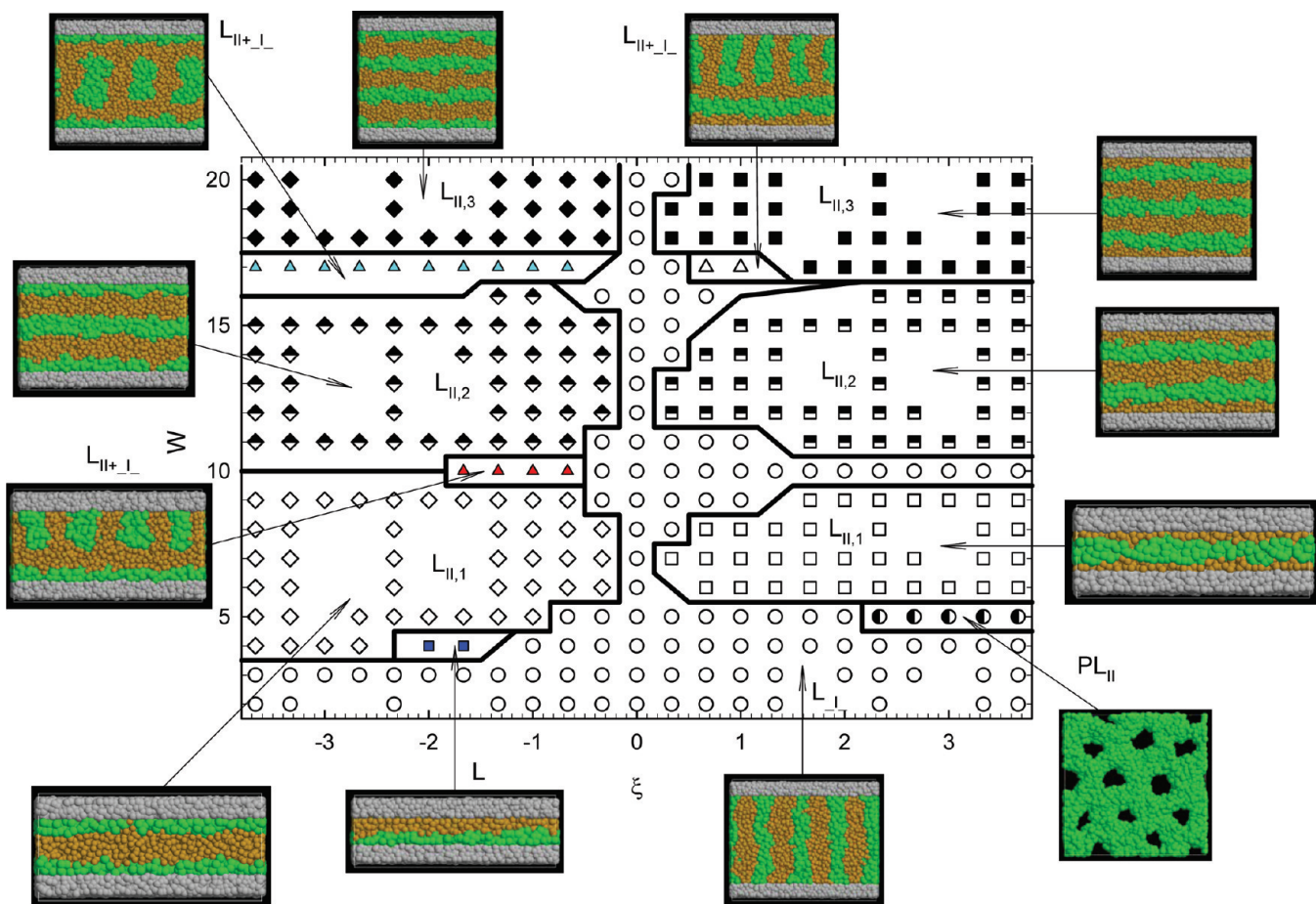


Figure 2. Phase diagram of the A_4B_6 system confined in planar slits, together with examples of simulation configurations for the particular phases. W is the slit width and ξ is the phobicity of the beads toward the walls. Symbols represent simulation results and solid lines indicate approximate microphase separation boundaries. The symbols refer to a perpendicular lamellar phase (L_{\perp}), a parallel lamellar phase with v parallel lamellae ($L_{\parallel,v}$), a parallel perforated lamellar phase (PL_{\parallel}), mixed lamellar phases ($L_{\parallel+\perp}$), and an adsorbed-layer phase (L). Green and gold spheres represent A- and B-beads, respectively, while gray spheres represent wall-beads.

were slightly tilted and/or undulated, which depended on the path to its final state. Furthermore, the coinciding chain structure properties differed among the various forms of the $L_{\parallel+\perp}$ phase. Taken together, these results provide evidence that PL_{\parallel} and L_{\perp} are stable phases, while $L_{\parallel+\perp}$ is a metastable phase associated with the first-order transformation from the L_{\perp} phase to the PL_{\parallel} phase. In addition, it is unlikely that a system of symmetric diblock copolymers confined between two identical walls with the same block-wall interactions would form a stable asymmetric phase with a parallel lamella close to one wall and perpendicular lamellae close to the other wall.

The pathway dependence of the PL_{\parallel} phase from the L_{\perp} phase (upon increasing the block-wall phobicity), and subsequent entrapment in the $L_{\parallel+\perp}$ phase bears resemblance to the simulation behavior of symmetric diblock copolymers systems under shear.^{33,34} When these simulations were started with lamellae oriented parallel to the shear plane, it was found that the parallel lamellar phase remains stable at small shear rates, while lamellae reorient into a perpendicular alignment at large shear rates. In a small range of shear rate values, the shear flow is not sufficient to fully reorient the lamellae, subsequently the systems become trapped with diagonally oriented lamellae. This behavior is a consequence of both the constraints induced by the periodic boundary conditions, as well as the slow, collective dynamics of

the diblock copolymers. The diagonal lamellar phase does not exist for real systems, where it has been shown theoretically³⁵ that the diagonal lamellar phase is metastable and corresponds to a local energy minimum. Upon formation of the diagonal lamellar phase, a high energy barrier to reorientation becomes present such that it is exceedingly unlikely to be overcome in a reasonable-length simulation without imposing an additional external field such as increasing the shear rate.^{34,35}

Analogous to these sheared systems, there is a small range of ξ values (bounded by the ξ values for the L_{\perp} and PL_{\parallel} phases) where the block-wall interactions are not sufficient to reorient perpendicular lamellae to parallel lamella, thus the system becomes trapped in an orientation that is comprised of a mixture of perpendicular and parallel lamellae. Similar to the diagonal-oriented lamellae of the sheared systems, the $L_{\parallel+\perp}$ phase is metastable and corresponds to a local energy minimum. For real copolymer systems, the phase transformation from the L_{\perp} phase into the PL_{\parallel} phase would occur at a unique value of ξ , where this value is bounded by the values of ξ for the L_{\perp} and PL_{\parallel} phases. Moreover, this transformation would be absent of the $L_{\parallel+\perp}$ phase altogether, which most likely is a simulation artifact.

To provide further insight into the stability of these lamellar morphologies for the A_5B_5 copolymers in slit width $W = 10$, we performed free-energy calculations that are summarized in

(33) Fraser, B.; Denniston, C.; Müser, M. H. *J. Chem. Phys.* **2006**, *124*, 104902.
(34) Lisal, M.; Brennan, J. K. *Langmuir* **2007**, *23*, 4809–4818.

(35) Fraser, B.; Denniston, C.; Müser, M. H. *J. Polym. Sci., Part B* **2005**, *43*, 970–982.

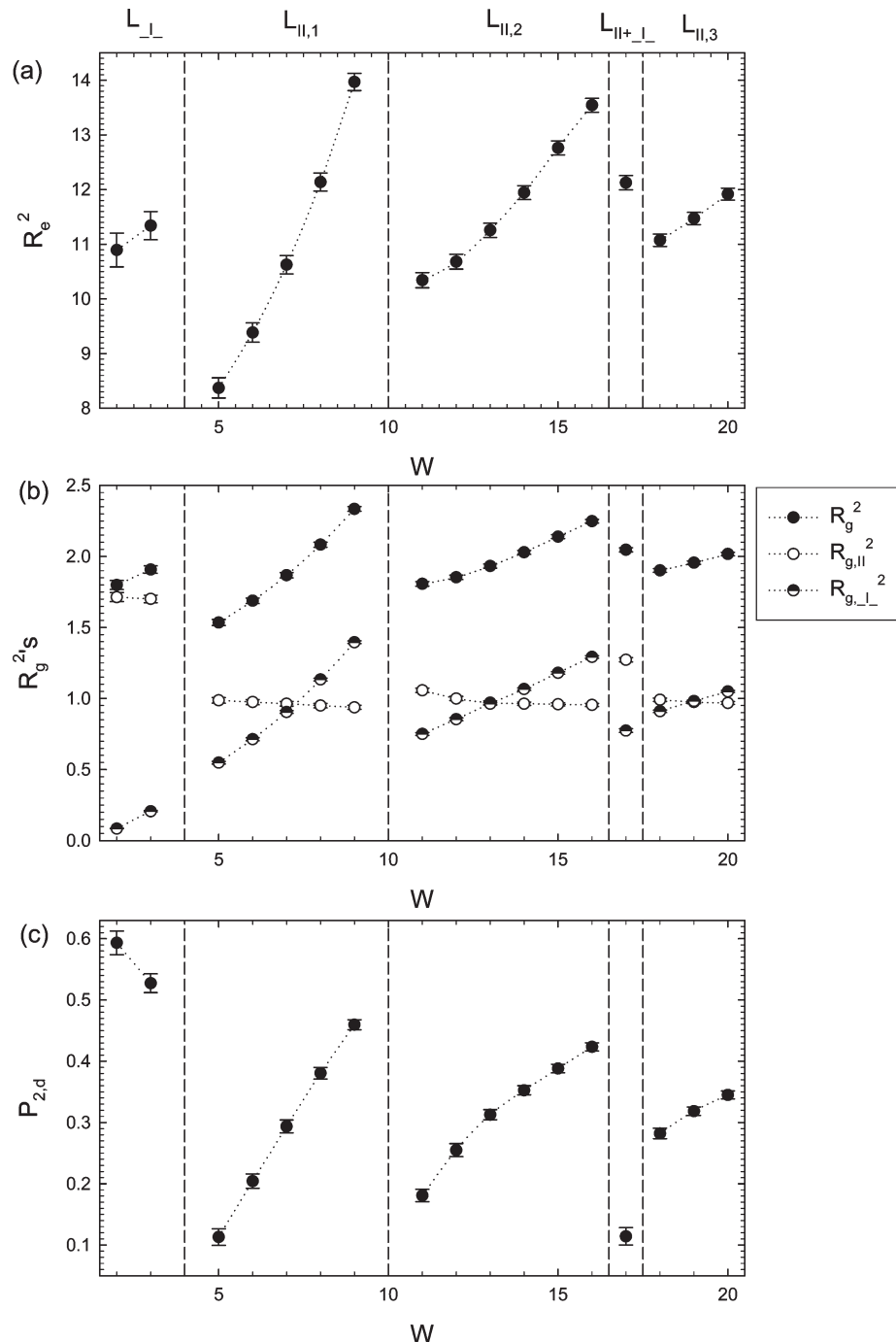


Figure 3. (a) The mean square end-to-end distance, R_e^2 , (b) the mean square radius-of-gyration, R_g^2 , and (c) the nematic order parameter, $P_{2,d}$, as a function of the slit width, W , for the A_4B_6 copolymers confined in planar slits, where $\xi = -7/3$. Error bars correspond to the statistical uncertainties of simulation data. Symbols represent simulation results, where dotted lines are drawn as a guide to the eye and vertical dashed lines mark approximate microphase separation boundaries. Symbols for particular phases are same as in Figure 2.

Figure 1, where $\beta F^{\text{ex}}/N$ is presented as a function of ξ . In Figure 1, F^{ex} increases with ξ within the L_{\perp} phase, where the increase becomes sharper when the L_{\perp} phase transforms into a $L_{\parallel+\perp}$ phase. The transformation from the $L_{\parallel+\perp}$ phase into parallel perforated lamellae is then accompanied by a sharp decrease of F^{ex} . The values of F^{ex} at the beginning of the PL_{\parallel} region do not differ significantly from those at the end of the L_{\perp} region, and F^{ex} only slightly increases with ξ within the PL_{\parallel} phase. Considering that the phase transformation from L_{\perp} to PL_{\parallel} should occur at a value of ξ within the $L_{\parallel+\perp}$ region, we can extrapolate F^{ex} from the L_{\perp} and PL_{\parallel} regions to the $L_{\parallel+\perp}$ region as shown in Figure 1.

The extrapolations clearly indicate that the calculated F^{ex} in the $L_{\parallel+\perp}$ region is indeed higher, providing further evidence that the $L_{\parallel+\perp}$ phase is metastable.

3.2. Slightly-Asymmetric Diblock Copolymers. Next, we consider the self-assembly of slightly asymmetric diblock copolymers in planar slits. Figure 2 displays a phase diagram for the A_4B_6 copolymers in various slit widths together with examples of simulation configurations for particular phases. Overall, the A_4B_6 system self-assembles into the following nanostructures: a perpendicular lamellar phase (L_{\perp}), a parallel lamellar phase with v parallel lamellae (denoted as $L_{\parallel,v}$), a parallel perforated lamellar

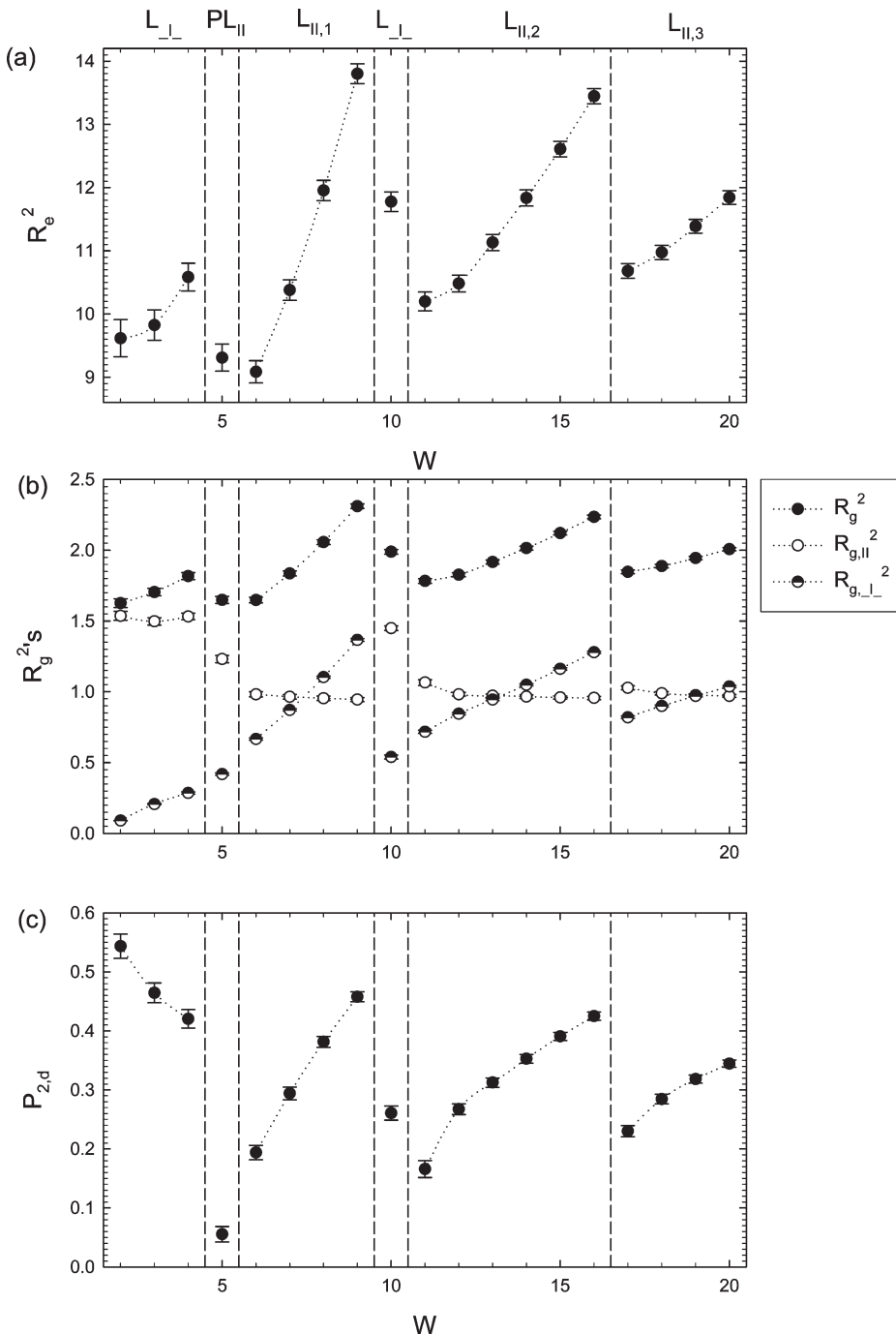


Figure 4. Figure caption same as Figure 3, except $\xi = 7/3$.

phase (PL_{\parallel}), mixed lamellar phases ($L_{\parallel+\perp}$), and an adsorbed-layer phase (denoted as L). Because of the asymmetry of the A_4B_6 copolymer, the phase diagram is also asymmetric. In the left portion of the phase diagram ($\xi < 0$), the phobicity of the longer B-blocks toward the walls increases with absolute values of ξ , while the shorter A-blocks exhibit affinity to the surfaces since $a_{Aw} = a_{AA}$. In the right portion of the phase diagram ($\xi > 0$), the situation is reversed, that is, the phobicity of the shorter A-blocks toward the surfaces increases with ξ and the longer B-blocks prefer the walls since $a_{Bw} = a_{BB}$. Therefore, in the left portion of the phase diagram, v refers to the number of B-lamellae, while in the right portion, v denotes the number of A-lamellae. Similar to the A_5B_5 phase diagram (cf. Figure 2 in ref 20), for narrow slit widths up to about 4, perpendicular lamellae are spontaneously

formed regardless of the interaction between the blocks and the walls due to steric reasons.

In the left portion of the phase diagram where $\xi \leq -2.5$, the system exhibits a succession of $L_{\perp}-L_{\parallel,1}-L_{\parallel,2}-L_{\parallel+\perp}-L_{\parallel,3}$ phases with increasing slit width. The mixed lamellar phase that exists in a narrow region around $W \approx 17$ is formed by perpendicular A-lamellae at the center of the slit and adsorbed A-layers on the opposite walls. For weaker phobicity of the B-blocks toward the walls (i.e., increasing ξ), two additional phases between L_{\perp} and $L_{\parallel,1}$ ($W \approx 4$), and between $L_{\parallel,1}$ and $L_{\parallel,2}$ ($W \approx 10$) are present. The adsorbed-layer phase between L_{\perp} and $L_{\parallel,1}$ consists of adsorbed A- and B-layers on opposite walls. The mixed lamellar phase between $L_{\parallel,1}$ and $L_{\parallel,2}$ is formed by perpendicular A-lamellae attached to one wall and an adsorbed A-layer on the other wall.

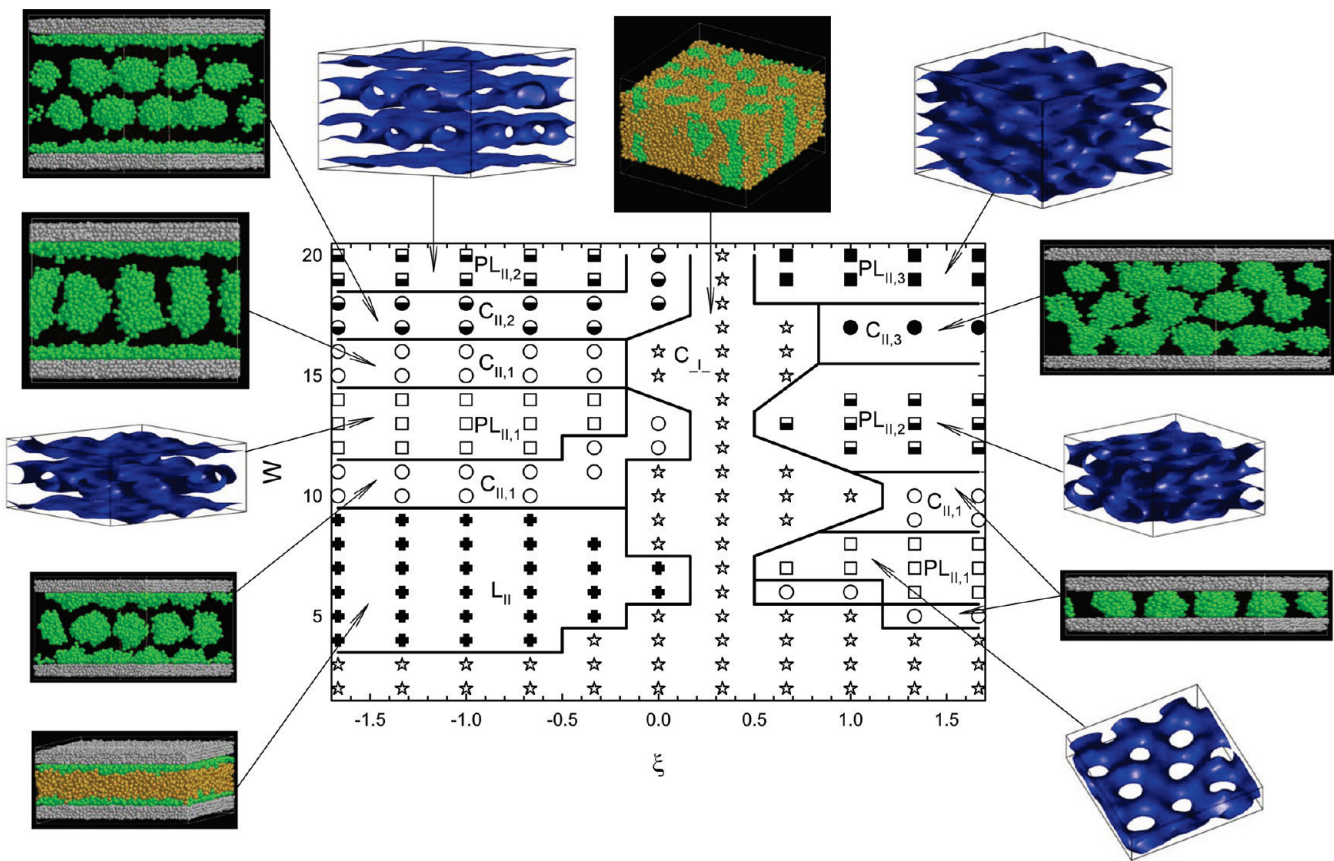


Figure 5. Phase diagram of the A_3B_7 system confined in planar slits, together with examples of simulation configurations for the particular phases. W is the slit width and ξ is the phobicity of the beads toward the walls. Symbols represent simulation results and solid lines indicate approximate microphase separation boundaries. The symbols refer to a perpendicular cylindrical phase (C_{\perp}), parallel cylindrical phases with v layers of cylinders ($C_{\parallel,v}$), a parallel lamellar phase (L_{\parallel}), and parallel perforated lamellar phases with v lamellae ($PL_{\parallel,v}$). Green and gold spheres represent A - and B -beads, respectively, while gray spheres represent wall-beads.

The appearance of the L and $L_{\parallel+\perp}$ phases suggests that direct transformations between the $L_{\parallel,v}$ and $L_{\parallel,v+1}$ orientations does not occur, rather they transition through these phases.

In the right portion of the phase diagram where $\xi \geq 2$, the system exhibits a succession of $L_{\perp}-PL_{\parallel}-L_{\parallel,1}-L_{\perp}-L_{\parallel,2}-L_{\parallel,3}$ phases with increasing slit width. Here, the phase diagram resembles the A_5B_5 phase diagram, where exceptions in the A_4B_6 phase diagram are the appearance of the PL_{\parallel} phase at $W \approx 4$ and the absence of the PL_{\parallel} phase at $W \approx 10$ for large values of ξ . This suggests that the asymmetry of the A_4B_6 copolymers does not play a significant role in this portion of the phase diagram. When the phobicity of the A -blocks toward the walls weakens, that is, $\xi < 2$, we observe the disappearance of the PL_{\parallel} phase along with more frequent occurrence of the perpendicular lamellar phases. In addition, there is a mixed lamellar phase between $L_{\parallel,2}$ and $L_{\parallel,3}$ ($W \approx 17$) formed by perpendicular A -lamellae attached to one wall and a parallel A -lamella close to the other wall. As in the case of the A_5B_5 system, when there is no preferential affinity of the A - or B -blocks toward the walls, the system self-assembles into a perpendicular lamellar phase for all slit widths.

Figures 3 and 4 show R_e^2 , R_g^2 s, and $P_{2,d}$ as a function of W for two particular values of phobicity, $\xi = -7/3$ and $7/3$, which provide further insight into the behavior of the A_4B_6 copolymer self-assembly. In narrow slits where the system forms perpendicular lamellae, the diblock copolymers become increasingly elongated in the perpendicular direction (i.e., R_e^2 and R_g^2 increase) and the system loses orientational order (i.e., $P_{2,d}$ decreases) as

W increases. This behavior is associated with a release of the steric constraint imposed by the confining walls. For $W > 4$ or 5 , the transformation into a particular parallel phase is accompanied by a dramatic elongation of the diblock copolymers in the perpendicular direction, as evidenced by the increase of R_e^2 , R_g^2 , and $P_{2,d}$ with increasing W within each $L_{\parallel,v}$ phase. As the slit width is increased, structural frustration of the diblock copolymers in the parallel lamella(e) is relieved by either formation of an additional parallel lamella or a reorientation of the parallel lamella(e) to form the transition phases described above, L_{\perp} or $L_{\parallel+\perp}$. For either of these occurrences, the diblock copolymers have collapsed upon themselves to minimize free-energy, while subsequently losing orientational order. As expected for $W > 4$ or 5 , the values of R_g^2 adopt distinct values for the $L_{\parallel,v}$ phases and for the transition phases, which do not depend on W within the parallel lamellar regions. This behavior implies that the parallel orientational order of the lamellae is maximized with respect to the slit width. For the other nonzero values of ξ shown in Figure 2, the conformational and system orientational-order behaviors are similar to those reported for $\xi = -7/3$ and $7/3$ but are not shown here. For the $\xi = 0$ case (also not shown here), we observed conformational and system orientational-order behaviors similar to the A_5B_5 system at $\xi = 0$; see Figure 3 in ref 20.

3.3. Highly-Asymmetric Diblock Copolymers. Next, we consider the self-assembly of highly asymmetric diblock copolymers in planar slits. Figure 5 shows a phase diagram for the A_3B_7 copolymers confined in various slit widths, along with examples of simulation configurations for particular phases. Overall, the

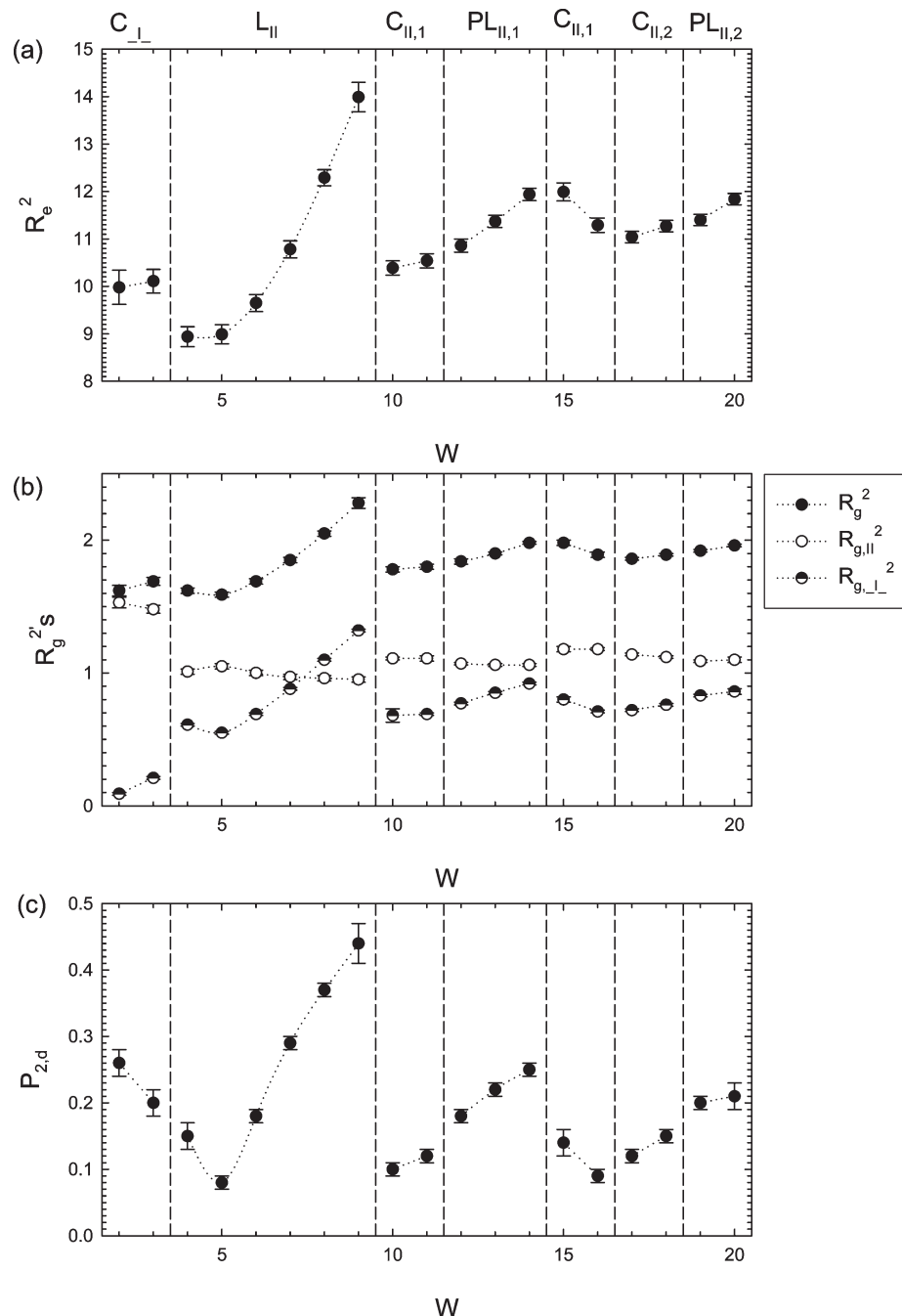


Figure 6. (a) The mean square end-to-end distance, R_e^2 , (b) the mean square radius-of-gyration, R_g^2 , and (c) the nematic order parameter, $P_{2,d}$, as a function of the slit width, W , for the A_3B_7 copolymers confined in planar slits, where $\xi = -4/3$. Error bars correspond to the statistical uncertainties of simulation data. Symbols represent simulation results, where dotted lines are drawn as a guide to the eye and vertical dashed lines mark approximate microphase separation boundaries. Symbols for particular phases are same as in Figure 5.

A_3B_7 system spontaneously forms the following nanostructures: a perpendicular cylindrical phase (denoted as C_{\perp}), parallel cylindrical phases with v layers of cylindrical domains (denoted as $C_{\parallel,v}$), a parallel lamellar phase (denoted as L_{\parallel}), and parallel perforated lamellar phases with v lamellae (denoted as $PL_{\parallel,v}$). Cylindrical and lamellar domains of the nanostructures are formed by the shorter A-blocks. Because of the asymmetry of the A_3B_7 copolymer, the phase diagram is also asymmetric. Similar to the A_4B_6 phase diagram, the phobicity of the longer B-blocks toward the walls increases with absolute values of ξ in the left portion of the phase diagram ($\xi < 0$), while the shorter A-blocks exhibit affinity to the surfaces since $a_{Aw} = a_{AA}$. In the right portion of the phase diagram ($\xi > 0$), the situation is again reversed and the phobicity

of the shorter A-blocks toward the surfaces increases with ξ and the longer B-blocks prefer the walls since $a_{Bw} = a_{BB}$. It was more difficult to determine the most probable nanostructures in the right portion of the phase diagram since it is more computationally challenging to stabilize structures with surfaces preferentially wet by the longer B-blocks than with surfaces preferentially wet by the shorter A-blocks in the left portion of the phase diagram.¹⁸ Hence, in Figure 5, we do not show data points that exhibited multiple or transient phases, i.e., data points for which different box sizes did not produce the same morphology.

Similar to the previous A_5B_5 and A_4B_6 systems, for narrow slit widths up to about 4 cylindrical domains adopt perpendicular orientation regardless of the interaction between the blocks and

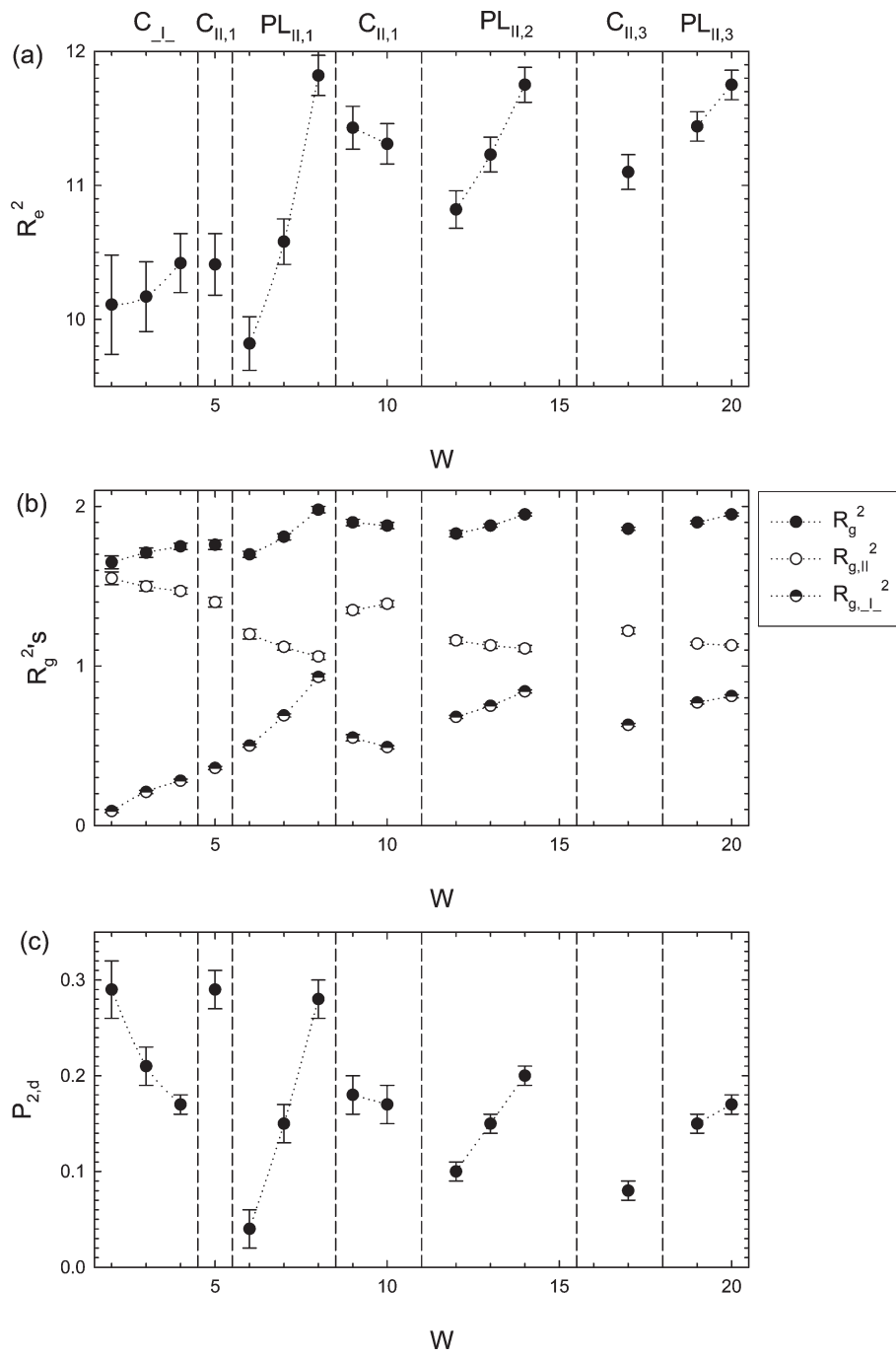


Figure 7. Figure caption same as Figure 6, except $\xi = 4/3$.

the walls due to steric reasons. In the left portion of the phase diagram when $\xi \leq -0.25$, the system displays a succession of $C-L_{\parallel}-C_{\parallel,1}-PL_{\parallel,1}-C_{\parallel,1}-C_{\parallel,2}-PL_{\parallel,2}$ phases with increasing slit width. The parallel cylindrical phases near $W = 10$, and those near $W = 15$ are slightly different. The $C_{\parallel,1}$ phases near $W = 10$ contain cylindrical domains with roughly circular cross sections, while those near $W = 15$ have cylindrical domains with oval cross sections. From Figure 5, it is evident that only a small increase in the slit width above $W = 16$ causes a separation of the cylindrical domains with oval cross sections, whereby two layers of cylindrical domains are formed leading to the $C_{\parallel,2}$ phases. In the right portion of the phase diagram when $\xi \geq 1$, the system shows a succession of $C_{\perp}-C_{\parallel,1}-PL_{\parallel,1}-C_{\parallel,1}-PL_{\parallel,2}-C_{\parallel,3}-PL_{\parallel,3}$ phases with increasing slit width. The parallel cylindrical and parallel

perforated lamellar phases that occur in the left and right portions of the phase diagram differ by the presence of an adsorbed A-layer on the confining surfaces. In the middle portion of the phase diagram ($-0.25 < \xi < 1$), we see a frequent occurrence of perpendicular cylindrical phases along with the appearance of some phases present in the left or right portions of the phase diagram. In contrast to the previous A_5B_5 and A_4B_6 systems that exhibited perpendicular orientations of the domains (lamellae) regardless of the slit width around $\xi = 0$, the A_3B_7 copolymers self-assemble into a perpendicular cylindrical phase for all slit widths ($W = 2$ to 20) around $\xi = 1/3$.

Figures 6 and 7 show R_e^2 , R_g^2 's, and $P_{2,d}$ as a function of W for two particular values of phobicity, $\xi = -4/3$ and $4/3$, which provide further insight into the behavior of the A_3B_7 copolymer

self-assembly. Both figures demonstrate that the transformation into a particular phase is accompanied by changes in the conformations of the A_3B_7 copolymers and system orientational order, where upon phase transitions, R_e^2 , R_g^2 's, and $P_{2,d}$ exhibit either abrupt changes in their values or changes in the slope of their dependence on W .

In Figure 6, the conformational behavior of chains within the C_{\perp} phase ($W = 2$ and 3) is only marginally affected by the change in W since R_e^2 and R_g^2 's do not vary significantly, while the system orientational order slightly decreases, as indicated by the behavior of $P_{2,d}$. The transformation into the L_{\parallel} phase with increasing W is accompanied by a dramatic elongation of the A_3B_7 copolymers in the perpendicular direction and an increase in system orientational order, as evidenced by the increase of R_e^2 , $R_{g,\perp}$, and $P_{2,d}$. Note that the values of $R_{g,\parallel}$ within the particular phases are nearly independent of W and the values of $R_{g,\parallel}^2$ are nearly the same for all parallel (L_{\parallel} , $PL_{\parallel,1}$, $PL_{\parallel,2}$, $C_{\parallel,1}$, and $C_{\parallel,2}$) phases. Here again, the parallel orientational order of the system appears to have maximized. As the slit width is further increased, structural frustration of the A_3B_7 copolymers in the L_{\parallel} phase is relieved by transformation into the parallel cylindrical phase. Upon further increase of W , the A_3B_7 copolymers again are elongated in the perpendicular direction and the system orientational order increases even when the $C_{\parallel,1}$ phase transforms into the $PL_{\parallel,1}$ phase. As W increases, the reappearance of the $C_{\parallel,1}$ phase (with cylindrical domains containing oval cross sections) allows for a smooth release of the chain stretching and a decrease of the system orientational order. The formation of two layers of cylindrical domains from the cylindrical domains with oval cross sections, and the subsequent transformation into the $PL_{\parallel,2}$ phase again, causes elongation of the A_3B_7 copolymers in the perpendicular direction and an increase in the system orientational order.

The conformational and system orientational-order behaviors shown in Figure 7 follow similar logic as those in Figure 6. The chains are stretched within the particular phases except when the $C_{\parallel,1}$ phase reappears between the $PL_{\parallel,1}$ and $PL_{\parallel,2}$ phases, which again allows for a nonabrupt release of the chain stretching. The system orientational order also increases within the particular phases except for the C_{\perp} phase and the reappearing $C_{\parallel,1}$ phase, where the system orientational order decreases with increasing W . However, in contrast to Figure 6, $R_{g,\parallel}^2$ exhibits some dependence on W within the particular phases indicating some chain stretching/shrinking in the parallel direction. For the other nonzero values of ξ shown in Figure 5, the conformational and system orientational-order behaviors are similar when compared to $\xi = -4/3$ and $4/3$, but are not shown here. For the $\xi = 1/3$ behavior (also not shown here), where the system self-assembles into the C_{\perp} phase regardless of slit width, we observed conformational and system orientational-order behaviors similar to the A_5B_5 system at $\xi = 0$; see Figure 3 in ref 20.

4. Conclusions

We performed DPD simulations of model lamellar- and cylinder-forming diblock copolymers confined in planar slits with the goal of systematically investigating and qualifying the competing effects of physical adsorption and confinement on the self-assembly. The DPD copolymer models can be considered as generic models for low-molecular-weight diblock copolymers such as the PS-PVP copolymer with average molecular weight 10 300 g mol⁻¹ at 300 K. We considered a wide range of slit widths (from 33.6 to 336 Å, or 2 to 20 in reduced units) and diblock copolymer bead–wall interactions from preferential affinity to strong phobicity. We determined the confined phase behavior by

analyzing equilibrium configurations in terms of bead-density profiles and isosurfaces, along with the coinciding characterization of the conformational behavior of the confined copolymers.

Depending on the slit width and the diblock copolymer bead–wall interaction, the symmetric and slightly asymmetric A_5B_5 and A_4B_6 systems primarily self-assembled into perpendicular and parallel lamellar phases with different number of lamellae. In addition, we found that the A_5B_5 system can also spontaneously form a parallel perforated lamellar phase in a narrow region of the phase diagram, where free-energy calculations provided further insight into the occurrence and relative stability of this morphology. Due to the slight asymmetry of the A_4B_6 copolymers, this system can also self-assemble into various mixed lamellar phases. We observed mixed lamellar phases with perpendicular lamellae either in the center of the slits or attached to one of the confining walls and accompanied by an adsorbed-layer(s) on the wall(s) or a parallel lamella close to the wall. The occurrence of the mixed lamellar phases is restricted to a few, narrow portions of the phase diagram. The highly asymmetric A_3B_7 system self-assembled not only into perpendicular and parallel cylindrical phases with different number of layers of cylindrical domains but also into noncylindrical structures such as parallel lamellae and parallel perforated lamellae with different number of lamellae. Overall, rich phase behavior unique to the considered confined conditions was observed that could be utilized for a plethora of nanoscale applications.³

Acknowledgment. The authors are grateful to Alexandr Maljevský (Institute of Chemical Process Fundamentals of the ASCR, v. v. i.) for insightful discussions. This research was supported by the Grant Agency of the Czech Republic (Grant 203/08/0094), by the Grant Programme of the Academy of Sciences of the Czech Republic “Nanotechnology for Society” (Project No. KAN400720701), by the Internal Grant Agency of the J. E. Purkinje University (Grants 53224 15 0008 01 and No. 53222 15 0006 01), and by the European Community under the seventh Framework Programme (Project COST TD0802/OC10053). This research was also sponsored by the Army Research Laboratory and was accomplished under Cooperative Agreement Number W911NF-10-2-0039. The views and conclusions contained in this document are those of the authors and should not be interpreted as representing the official policies, either expressed or implied, of the Army Research Laboratory or the U.S. Government.

APPENDIX

This appendix provides details of our DPD simulations of confined diblock copolymer systems and the connection of the models to real systems. Also included are details regarding the calculation of the chemical potential and the spreading pressure for the free-energy calculations.

A. DPD Simulation of Diblock Copolymers Confined between Parallel Walls. In typical DPD fashion, we model a diblock copolymer as a flexible chain of point beads connected by harmonic springs that represent lumps of the real chain comprised of several monomer segments.^{29,30} The DPD diblock copolymer A_nB_m therefore consists of A_n - and B_m -blocks connected end-to-end with n and m A- and B-beads, respectively. Confining walls are modeled by creating dense layers of DPD beads that represent several atoms, where the DPD beads are arranged on a lattice.³⁶ The density of the wall layers must be sufficiently large to avoid

(36) Malfreyt, P.; Tildesley, D. J. *Langmuir* 2000, 16, 4732–4740.

penetration of the diblock copolymer beads into these confining walls.

All DPD beads are defined by a mass m_i , position \mathbf{r}_i , and velocity \mathbf{v}_i , and interact with each other via a pairwise, two-body, short-ranged force \mathbf{F} that is written as the sum of a conservative force \mathbf{F}^C , dissipative force \mathbf{F}^D , and random force \mathbf{F}^R

$$\mathbf{F}_{ij} = \mathbf{F}_{ij}^C + \mathbf{F}_{ij}^D + \mathbf{F}_{ij}^R \quad (\text{A-1})$$

For the diblock copolymer chains, \mathbf{F}^C includes a soft repulsion force, \mathbf{F}^{Cr} , acting between bonded and nonbonded beads and a harmonic spring force, \mathbf{F}^{Cs} , acting between bonded beads in a chain. For a wall-bead w , \mathbf{F}^C contains, in addition to \mathbf{F}^{Cr} , a wall force \mathbf{F}^{Cw} that tethers a wall-bead to its initial position \mathbf{r}_w . Expressions for \mathbf{F}^{Cr} , \mathbf{F}^{Cs} , and \mathbf{F}^{Cw} are given by

$$\mathbf{F}_{ij}^{Cr} = \begin{cases} a_{ij} \left(1 - \frac{r_{ij}}{r_c} \right) \frac{\mathbf{r}_{ij}}{r_{ij}} & r_{ij} < r_c \\ 0 & r_{ij} \geq r_c \end{cases} \quad (\text{A-2})$$

$$\mathbf{F}_{ij}^{Cs} = -K_s(r_{ij} - r_0) \frac{\mathbf{r}_{ij}}{r_{ij}} \quad (\text{A-3})$$

and

$$\mathbf{F}_i^{Cw} = -K_w(\mathbf{r}_i - \mathbf{r}_{w,i}) \quad (\text{A-4})$$

respectively. In eqs A-2 to A-4, a_{ij} is the maximum repulsion between bead i and bead j , $\mathbf{r}_{ij} = \mathbf{r}_i - \mathbf{r}_j$, $r_{ij} = |\mathbf{r}_{ij}|$, r_c is the cutoff radius, K_s is the spring constant, r_0 is the equilibrium spring length and K_w is the wall-bead tethering constant.

The remaining two forces \mathbf{F}^D and \mathbf{F}^R are given by

$$\mathbf{F}_{ij}^D = -\gamma_{ij}\omega^D(r_{ij}) \left(\frac{\mathbf{r}_{ij} \cdot \mathbf{v}_{ij}}{r_{ij}} \right) \frac{\mathbf{r}_{ij}}{r_{ij}} \quad (\text{A-5})$$

$$\mathbf{F}_{ij}^R = \sigma_{ij}\omega^R(r_{ij}) \frac{\zeta_{ij}}{\sqrt{\Delta t}} \frac{\mathbf{r}_{ij}}{r_{ij}} \quad (\text{A-6})$$

where $\omega^D(r_{ij})$ and $\omega^R(r_{ij})$ are weight functions that vanish for $r_{ij} \geq r_c$, γ_{ij} is the friction coefficient, σ_{ij} is the noise amplitude, $\mathbf{v}_{ij} = \mathbf{v}_i - \mathbf{v}_j$, ζ_{ij} is a Gaussian random number with zero mean and unit variance that is chosen independently for each pair of interacting beads, and Δt is the time step.

Español and Warren showed³⁷ that the system samples the canonical ensemble and obeys the fluctuation-dissipation theorem if the following relations hold

$$\omega^D(r_{ij}) = [\omega^R(r_{ij})]^2 \quad (\text{A-7})$$

$$\sigma_{ij}^2 = 2\gamma_{ij}k_B T \quad (\text{A-8})$$

where T is the temperature and k_B is Boltzmann's constant. $\omega^D(r_{ij})$ and $\omega^R(r_{ij})$ are typically chosen³⁰ as

$$\omega^D(r_{ij}) = [\omega^R(r_{ij})]^2 = \begin{cases} \left(1 - \frac{r_{ij}}{r_c} \right)^2 & r_{ij} < r_c \\ 0 & r_{ij} \geq r_c \end{cases} \quad (\text{A-9})$$

The confining walls are comprised of four layers of DPD beads arranged on a face-centered-cubic lattice (following the work of Malfreyt and Tildesley³⁶) with a wall density approximately 3.5ρ , where ρ is the bead number-density. The calculated A- and B-bead density profiles confirmed that this wall density avoids penetration of the diblock copolymer beads into the confining walls. Since the wall beads are tethered to their lattice positions by stiff harmonic springs, no additional repulsion interactions between the wall-beads themselves are needed, therefore we set $a_{ww} = 0$.

The evolution of DPD beads in time t is governed by Newton's equations of motion

$$\begin{aligned} \frac{d\mathbf{r}_i}{dt} &= \mathbf{v}_i(t) \\ m_i \frac{d\mathbf{v}_i}{dt} &= \mathbf{f}_i(t) = \sum_{j \neq i} (\mathbf{F}_{ij}^C + \mathbf{F}_{ij}^D + \mathbf{F}_{ij}^R) \end{aligned} \quad (\text{A-10})$$

B. Top-Down Mapping of DPD Diblock Copolymer Models. To determine the values of a_{ij} , we used expressions obtained by Groot and Warren that map DPD polymer models onto Flory-Huggins-type models.³⁰ Groot and Warren derived the following expressions for the like-interactions

$$\frac{a_{AA}r_c}{k_B T} \equiv \frac{a_{BB}r_c}{k_B T} = \frac{75}{\rho r_c^3} \quad (\text{B-1})$$

and for the unlike-interactions

$$\frac{a_{AB}r_c}{k_B T} = \frac{a_{BB}r_c}{k_B T} + a_1 \left[1 + \frac{a_2}{(n+m)^{a_3}} \right] \chi_{AB}^{\text{eff}}(T) \quad (\text{B-2})$$

where χ_{AB}^{eff} is the effective Flory-Huggins interaction parameter, and a_1, a_2 , and a_3 are constants dependent on ρr_c^3 ; for example, $a_1 = 3.27$, $a_2 = 3.9$, and $a_3 = 0.51$ when $\rho r_c^3 = 3$,²⁴ which is used in this work.

The DPD models of symmetric and asymmetric diblock copolymers A_5B_5 , A_4B_6 , and A_3B_7 can be mapped onto real symmetric and asymmetric diblock copolymers by establishing physical values for r_c , m_{DPD} , and χ_{AB}^{eff} , using a top-down coarse-graining approach.³⁸ We demonstrate this mapping procedure using a low molecular-weight diblock copolymer, poly(styrene-*b*-2-vinylpyridine) (PS-PVP), with an average molecular weight of 10 300 g mol⁻¹. Assuming that the DPD diblock copolymers correspond to flexible Gaussian chains comprised of Kuhn's segments,³⁹ the number of monomers defined by a Kuhn segment, C_∞ , was estimated using the structural-relation method⁴⁰ with $C_\infty 9.9$ for both the PS and PVP blocks. Defining m_{mon} and V_{mon} as the average mass and average volume of the PS and PVP monomers, respectively, the mass and volume of a DPD bead was determined from $m_{DPD} \approx C_\infty m_{\text{mon}} \approx 1030$ g mol⁻¹ and $V_{DPD} \approx C_\infty V_{\text{mon}} \approx 1570 \text{ \AA}^3$, respectively. The value of r_c was defined as the side of a cube with an average number of beads corresponding to ρ , that is

$$r_c = (\rho V_{DPD})^{1/3} \quad (\text{B-3})$$

where we obtained for the PS-PVP system $r_c \approx 16.8 \text{ \AA}$. The value of χ_{AB}^{eff} can then be determined using the solubility parameters of

(38) Chennamsetty, N.; Bock, H.; Lísal, M.; Brennan, J. K. An Introduction to Coarse-Graining Approaches: Linking Atomistic and Mesoscales. In *Process Systems Engineering: Molecular Systems Engineering*; Adjiman, C., Galindo, A., Eds.; Wiley-VCH: Weinheim, 2010; Vol. 6.

(39) Rubinstein, M.; Colby, R. H. *Polymer Physics*; Oxford University Press: London, 2006.

(40) Bicerano, J. *Prediction of Polymer Properties*; Marcel Dekker: New York, 2002.

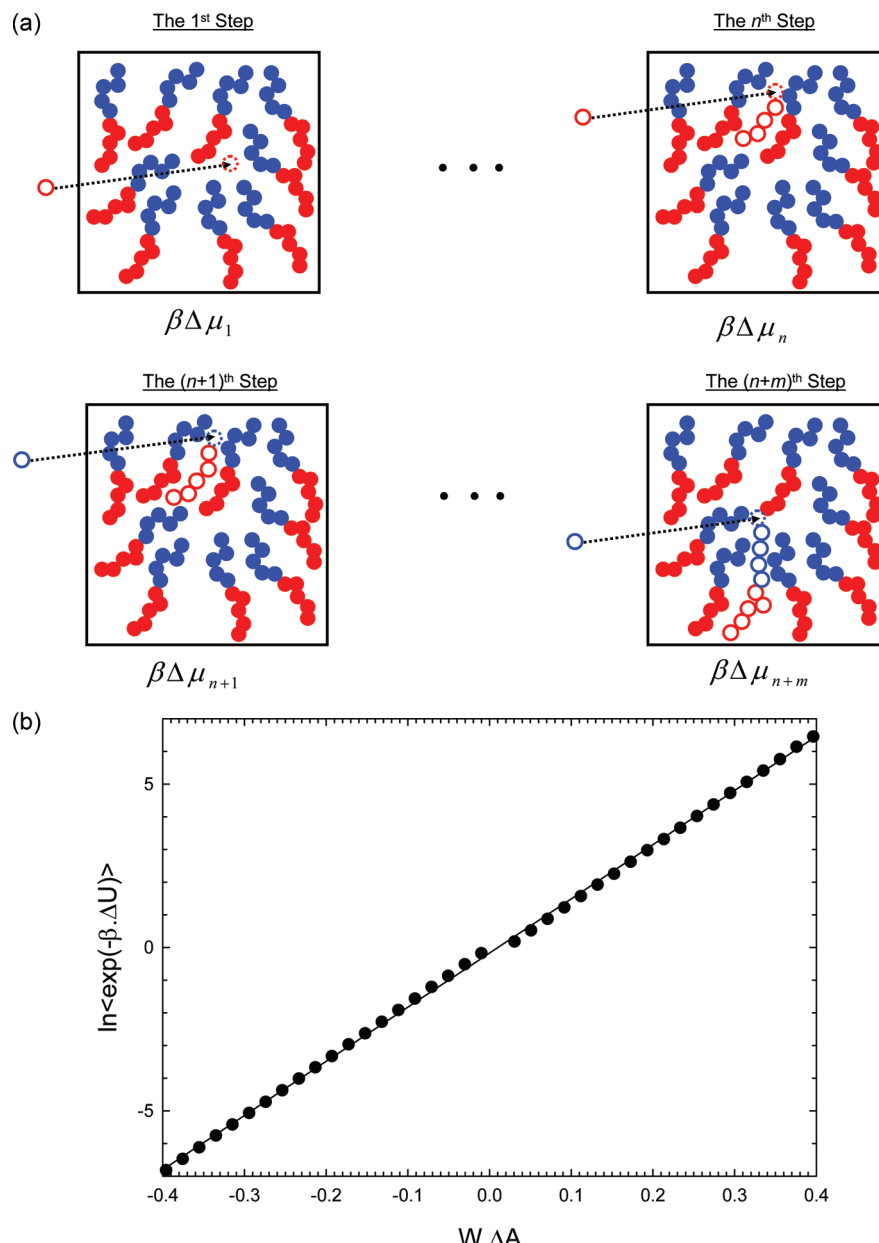


Figure 8. (a) Schematics of the chain-increment method used to calculate the configurational chemical potential of the diblock copolymers. (b) Illustrative calculation of Π^{ex} by extrapolating the ratio in eq C-3 to $\Delta A = 0$ (solid line); W is the slit width. Circles are the raw simulation data.

the A(PS)- and B(PVP)-beads, δ_A and δ_B ,⁴¹ from the expression

$$\chi_{AB}^{\text{eff}} = \frac{V_{\text{DDP}}}{k_B T} (\delta_A - \delta_B)^2 \quad (\text{B-4})$$

For the PS-PVP system, the structural-relation method⁴⁰ gives $\delta_A = 19.80 (\text{Jcm}^3)^{1/2}$ and $\delta_B = 22.12 (\text{Jcm}^3)^{1/2}$, so that when $T = 300 \text{ K}$ we obtain $\chi_{AB}^{\text{eff}} \approx 2$.

C. Determination of Chemical Potential and Spreading Pressure. The value of μ^{ex} in eq 8 was determined by the chain-increment method, which is based on the insertion of test beads onto the ends of a polymer and is applicable for any chain length at liquid-like densities.^{42,43} For the A_nB_m system, the technique

involves a set of independent simulations of a system comprising N full A_nB_m chains and one partial chain, where a test bead A or B is inserted onto the end of the partial chain. In the first simulation, the length of the partial chain is zero, i.e., the test bead is inserted randomly into the system. In the 2nd to $(n+m)$ th simulations, the partial chain corresponds to $A_1, A_2, \dots, A_n, A_nB_1, \dots, A_nB_{m-1}$, respectively. The test bead is inserted randomly on a sphere with a radius generated from the harmonic spring distribution³¹ and centered on the end bead of the partial chain. The test-bead insertions provide the incremental chemical potentials that can be evaluated using the Widom expression⁴⁴ as

$$\beta\Delta\mu_j^{\text{ex}} = -\ln\langle\exp(-\beta U_j^{\text{Cr}})\rangle \quad (\text{C-1})$$

(41) Prausnitz, J. M.; Lichtenthaler, R. N.; de Azevedo, E. G. *Molecular Thermodynamics of Fluid-Phase Equilibria*, 3rd Ed.; Prentice-Hall International Inc.: New York, 1999.

(42) Kumar, S. K.; Szleifer, I.; Panagiotopoulos, A. Z. *Phys. Rev. Lett.* **1991**, *66*, 2935–2938.

(43) Spyriouni, T.; Economou, I. G.; Theodorou, D. N. *Macromolecules* **1997**, *30*, 4744–4755.

(44) Widom, B. *J. Phys. Chem.* **1982**, *86*, 869–872.

where $\beta = 1/(k_B T)$ and $U_j^{\text{Cr}} = \Sigma_{k \neq j} u_{jk}^{\text{Cr}}$ is the energy of test-bead j and j and

$$u_{jk}^{\text{Cr}} = \begin{cases} \frac{a_{jk}}{2} r_c \left(1 - \frac{r_{jk}}{r_c}\right)^2 & r_{jk} < r_c \\ 0 & r_{jk} \geq r_c \end{cases} \quad (\text{C-2})$$

In eq C-2, a_{jk} is the maximum repulsion between test-bead j and bead k , and r_{jk} is their separation distance. The value of μ^{ex} corresponding to the insertion of the complete A_nB_m chain into the system is then given as a sum of $\Delta\mu_j^{\text{ex}}$, that is

$$\beta\mu^{\text{ex}} = \sum_{j=1}^{n+m} \beta\Delta\mu_j^{\text{ex}} \quad (\text{C-3})$$

The chain-increment method is schematically outlined in Fig. 8a.

The value of Π^{ex} in eq 8 is calculated using the virtual-parameter-variation (VPV) method of Vörtler and Smith.⁴⁵

(45) Vörtler, H. L.; Smith, W. R. *J. Chem. Phys.* **2000**, *112*, 5168–5174.

Π^{ex} is defined by

$$\beta\Pi^{\text{ex}} = -\frac{1}{W} \left(\frac{\partial\beta F^{\text{ex}}}{\partial A} \right)_{N,\beta,W} \quad (\text{C-4})$$

where the VPV method evaluates $(\partial\beta F^{\text{ex}}/\partial A)_{N,\beta,W}$ using the virtual changes of A as

$$\left(\frac{\partial\beta F^{\text{ex}}}{\partial A} \right)_{N,\beta,W} = -\lim_{\Delta A \rightarrow 0} \frac{\ln\langle \exp(-\beta\Delta U) \rangle}{\Delta A} \quad (\text{C-5})$$

and where $\Delta U = U(A + \Delta A) - U(A)$ is the change in the configurational energy U due to a change in the cross-sectional surface area A , ΔA . The VPV method involves a DPD simulation of A_nB_m chains in a slit accompanied by trial changes of A , typically after each time step. Each such trial consists of (i) a random change A to $A + \Delta A$, (ii) calculation of the Boltzmann factor $\exp(-\beta\Delta U)$, and (iii) recording the values of $\exp(-\beta\Delta U)$ in equal-sized bins of an A histogram according to ΔA . The value of the ratio in eq C-5 is evaluated using a linear regression of $\exp(-\beta\Delta U)$ on ΔA near $\Delta A = 0$, as shown in Figure 8b.